ChemPhotoChem

Research Articles
doi.org/10.1002/cptc.202300043

Chemistry Europe
European Chemical Societies Publishing

www.chemphotochem.org

Electron-Donating and Electron-Withdrawing Subunit Effects on Coumarin-BODIPY Dyads: Optical and Electrochemical Properties and Molecular Interactions

Baybars Köksoy,*[a] Mücahit Özdemir,[b] Sinem Altınışık,[c] Yunus Zorlu,[d] Bahattin Yalçın,[b] Mahmut Durmuş,[d] and Sermet Koyuncu*[c]

In this study, a series of coumarin-BODIPY molecules were synthesized using a Sonogashira cross-linking reaction. The effects of electron withdrawing and electron donating moieties on electrochemical and optical properties were supported by results of density functional theory calculations, and energy transfer mechanisms were investigated. The band gap value decreased from 2.0 eV to 1.6 eV due to reversible oxidation of the extra dimethylamino subunit at lower potential. Besides, characteristics of the crystal structures were investigated with single-crystal X-ray diffraction, and crystallinity was supported by differential scanning calorimetry. In addition, when the thin film surface morphologies were examined, it was clearly observed that the *N*,*N*-dimethylamino group on the coumarin-BODIPY dyad (**B3**) formed large-scale domains due to its crystalline behavior. As a result, Förster-type energy transfer was observed for coumarin-BODIPY dyads containing different electron withdrawing and donating subunits.

Introduction

Fluorescence resonance energy transfer (FRET) is a photophysical process that involves the transfer of excitation energy from an electronically excited fluorescent "donor" molecule to an "acceptor" molecule through a long-range dipole-dipole interaction.[1–3] The distance between the donor and the acceptor has a strong effect on the efficiency of energy transfer.[4–6] Furthermore, according to classical FRET theory, the donor structure must have a high quantum yield (Φ) to enhance the process efficiency.[7,8] This critical mechanism, which is located between two interacting fluorophores, is used in a variety of advanced applications, including (bio)sensors, energy harvesting, and light-emitting diodes.[9–12]

BODIPY (4,4-difluoro-4-bora-3a,4a-diaza-s-indacene) is a highly versatile fluorophore that exhibits a high absorption coefficient, thermal and photochemical stability, high fluorescence quantum yield, and spectral properties that can be tuned to the near-infrared (NIR) region through structural modifications.[13–15] A typical BODIPY chromophore center's absorption and emission wavelengths range from 470 to 530 nm.[16] The introduction of aryl, vinyl, styryl, and other substituents in the 3- or 5-carbon chain moves the BODIPY emission to a longer wavelength by extending the π-conjugation. BODIPY derivatives can be energy donors or acceptors in various energy transfer systems due to this structural adjustment.[17] Two significant disadvantages of the BODIPY derivatives are their low UV absorption and small Stokes shifts, which allow for undesirable re-absorption/re-emission processes.[18]

Coumarins are a notable class of organic compounds used as fluorescent dyes. Amino and hydroxycoumarin derivatives being particularly important due to their photophysical properties being controlled by internal charge transfer (ICT) upon light absorption. Furthermore, simple amino and hydroxycoumarins are characterized by their ability to absorb and emit light in the UV/blue-edge spectral region.[19] The intricate synthesis process, chemical instability, and the challenge of incorporating all desired photophysical properties into a single organic dye have prompted the idea of merging two different dyes with distinct photophysical properties into a hybrid dye with improved photophysical characteristics.[20]

The combination of two chromophore moieties (coumarin-BODIPY) provides excellent spectrally complementary and photophysical properties.[18,21,22] Of the many functional dyes employed to develop multi-chromophore structures, coumarin and BODIPYs are ideal not only for constructing and guaranteeing the electrical/optical response, but also for serving as molecular building blocks to control the self-assembly of highly organized supramolecular materials.[23] Lee *et al.* obtained a fluorescent dye via binding the phenyl bridged donor ethyl-

[a] *Asst. Prof. Dr. B. Köksoy*
Department of Chemistry
Bursa Technical University
16310 Bursa (Türkiye)
E-mail: baybars.koksoy@btu.edu.tr
[b] *M. Özdemir, Prof. Dr. B. Yalçın*
Department of Chemistry
Marmara University
34722 Kadikoy, Istanbul (Türkiye)
[c] *S. Altınışık, Prof. Dr. S. Koyuncu*
Department of Chemical Engineering
Canakkale Onsekiz Mart University
17100 Canakkale (Türkiye)
E-mail: skoyuncu@comu.edu.tr
[d] *Prof. Dr. Y. Zorlu, Prof. Dr. M. Durmuş*
Department of Chemistry
Gebze Technical University
41400 Kocaeli (Türkiye)

Supporting information for this article is available on the WWW under https://doi.org/10.1002/cptc.202300043

aminocoumarin to the BODIPY core from the meso position and used as a membrane-selective chemosensor in the endoplasmic reticulum.[24] Bai *et al.* coupled the 7-diethylamino donor coumarin directly from the meso position to the BODIPY dye by coumarin/BODIPY hybridization and obtained polar fluorescent sensors by examining its optical properties in detail.[25] Esnal *et al.* synthesized the coumarin/BODIPY hybrids using hydroxy and aminocoumarin derivatives and obtained photostable dye lasers for UV irradiation. They suggested that the aminocoumarin/BODIPY dyes are obtain as more red-shifted bright emission, while hydroxycoumarin/BODIPY pairs to increase fluorescence performance.[18] Bochkov *et al.* synthesized the asymmetric coumarin-BODIPY pairs directly fused to BODIPY compounds from 2nd or 6th carbon atom. According to this study, the absorption and emission properties were strongly influenced by the substitution on the coumarin moiety. Coumarin dyes containing donor diethylamino subgroup exhibited near-infrared emission with mega-Stokes shifts and good fluorescent quantum yields.[19] Wang *et al.* combined 7-diethylaminobenzathiazolcoumarin and BODIPY dyes to form an iridium complex and obtained a broadband and powerful visible light-absorbing photosensitizer, using these BODIPY/coumarin complexes for photocatalytic hydrogen evaluation, and reported excellent results.[26]

Based on this information, herein we aimed to investigate in detail the effect of different electron withdrawing and electron donating groups on the FRET mechanism of the coumarin-BODIPY structure, which can transfer energy as a result of absorption-emission band overlap.[18,27] As a result of the detailed characterization, the pendant group both influences on the crystalline characteristics of the structure and also the electrochemical-optic behaviors. It has been concluded that these molecules with high FRET energy transfer efficiency can be quite suitable for optoelectronic applications (such as OLED, OPV, OFET, etc.).

Results and Discussion

Synthesis and Characterization

Scheme 1 shows the synthetic methodology of the propargylated-coumarin derivatives (**C1**, **C2** and **C3**) and coumarin-BODIPY dyads **B1**-**B3**.

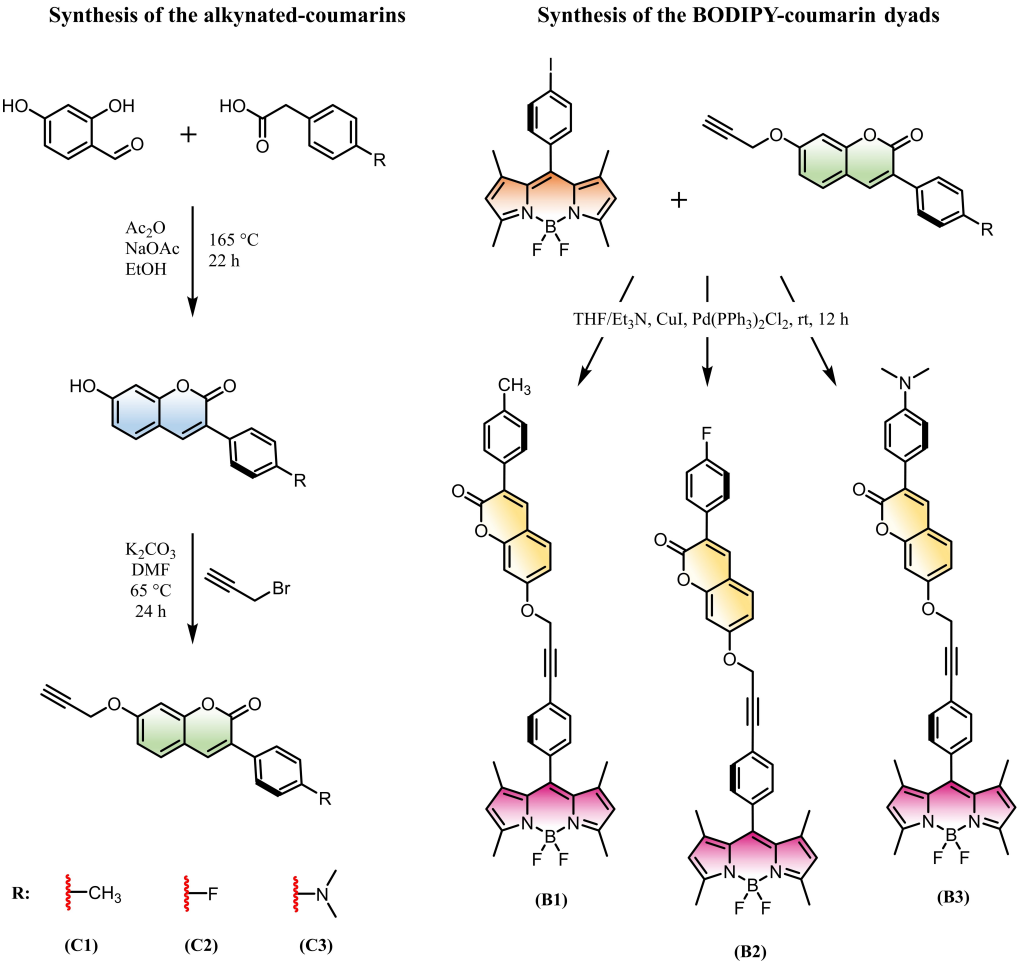

Scheme 1. Synthetic pathway for the preparation of propargylated-coumarins (**C1**-**C3**) and coumarin-BODIPY dyads (**B1**-**B3**).

The target compounds were obtained from reactions of a BODIPY derivative bearing an iodo group on its meso position and coumarin derivatives bearing a terminal alkynyl group. The disappearance of the peaks for the –C≡C–H group on the terminal alkyne coumarin derivatives in their FT-IR spectra (3288–3240 cm^{-1}), and the disappearance of the peak at approximately 2.60 ppm in the ^{1}H-NMR spectra of these coumarin derivatives (**C1**-**C3**) are important evidences that the compounds **B1**-**B3** were obtained. However, in the FT-IR spectra of the three target compounds, the C=O vibration peak for the lactone ring of the coumarins were observed at approximately 1720 cm^{-1}, and these groups were observed at 163.9, 160.9 and 163.9 ppm in the ^{13}C-NMR spectra of these compounds (**B1**-**B3**).

The ^{1}H-NMR spectra also consist of data to prove that the target compounds were synthesized. The hydrogen atom at the C-4 position of the coumarins was observed at 7.79, 7.79 and 7.72 ppm values for the three compounds (**B1**-**B3**), respectively. In addition, the specific pyrrole–H atoms of the BODIPYs were observed at approximately 6.00 ppm. Other aromatic and aliphatic–H atoms are also consistent with the literature.

Considering the mass spectra, the main peaks for coumarin-BODIPY target dyads were observed at 612.4, 616.22 and 641.8 m/z, respectively. The target coumarin-BODIPY dyad structures are demonstrated to be accurate when all characterization techniques are taken into account.

Single-Crystal Structures and Intermolecular Interactions

The BODIPY (**B1, B2** and **B3**) crystals were investigated by X-ray crystallography analysis to gain deep insight into the spatial arrangement of the molecules, crystal packing, and intermolecular interactions. Crystallographic data and refinement details of the data collection are given in Table S1. The suitable red crystals of **B1**, **B2** and **B3** for single-crystal X-ray diffraction analysis were grown by diffusion of hexane into a dichloromethane solution at room temperature. The conjugated backbone (C_9BN_2) of BODIPY in **B1**-**B3** exhibits a substantially planar molecular configuration with negligible interplanar twists and the dihedral angle between the meso-phenyl group and the boron-dipyrromethene π-core are positioned almost perpendicular (88.41(15)° for **B1**, 81.31(13)° for **B2**, 86.1(3)° for **B3**) to each other due to the steric hindrance of the attached methyl groups.[28–30] The B–F bond lengths and F–B–F, N–B–N, and N–B–F bond angles are in agreement with the values observed for the BODIPY compounds published in the literature.[31–33] The coumarin backbone attached *via* ethynyl unit at meso-position is tilted with respect to BODIPY frame with the inter-ring dihedral angles θ = 34.26(9)° for **B1**, θ = 70.13(9)° for **B2** and θ = 59.46(18)° for **B3** and this indicate that the conjugation does not extend over the entire molecular system since a flexible C–O–C bond is present (Figure 1-A1, A2 and A3). In **B1**, despite the π-conjugated structure of BODIPY, the π-π interactions were found to be weak interactions above the 4 Å distance. Two molecules in **B1** are linked to each other through C–H···π(ethynyl) (d(H···π) = 2.951 Å), C–H···π(phenyl) (d(H···π) = 2.655 Å) and –C=O(δ−)···π(phenyl) (d(C=O(δ−)···π = 3.602 Å) contacts (Figure 1-C1). Also, it should be noted that the molecular conformation of the precursor **C1** (Figure 1-B1) has not undergone any change in the **B1** compound.

The strong local dipoles of –C=O groups in alkynated-coumarin of **B1** were found to align anti-parallel to each other with slight slip stacks as observed in the precursor coumarin compound (Figure 1-B1, D1, E1 and F1). This indicates the presence of dipole-dipole interactions, which may overcome the dominating π-π interactions (face-to-face), which may prevent aggregation through a mechanism that involves π-π stacking interactions. In **B2**, similar to **B1**, the coumarin rings are stacked slipping over each other, in which the π-π interaction distance was observed to be quite weak above the 4 Å distance.

The short intermolecular –CH/F interactions are found to be effective adjacent molecules (4 interactions per molecule; Figure 1-B2) along the *c*-axis, which resulted in the formation of infinite one-dimensional chains. These chain constructions are expanded into a 3D supramolecular network by a combination of –CH/O interactions (6 interactions per molecule; Figure 1-C2). The ethynyl unit is almost orthogonal to the coumarin backbone in **C3** compound (Figure 1-B3), but in the **B3** (Figure 1-A3), it is seen that they are completely in the same plane with the coumarin framework.

Unlike **B1** and **B2**, very strong π-π stacking interactions (d(π···π) = 3.518(4) Å–3.858(4) Å) between the coumarin moieties in the solid-state structure of the **B3** molecule form the π-dimer structure of **B3** (Figure 1-C3), which possibly favoring charge carrying properties in the solid state. Similar to **C1** compound, the local dipoles of –C=O groups in **C3** were found to align anti-parallel to each other with slight slip stacks through –C=O(δ−)···π(coumarin) interactions (Figure 1-D3). The major intermolecular contacts governing the crystal structure are identified as the intermolecular C–H···O interactions (a: d(H···O) = 2.589 Å, b: d(H···O) = 2.483 Å).

Photophysical Properties

Absorption, fluorescence, and 3D-fluorescence measurements of all synthesized coumarins (**C1**-**C3**) and coumarin-BODIPYs (**B1**-**B3**) were measured in dichloromethane and all data are given in Table 1. The main transition band, which represents the transition from S0 to S1 in the UV-Vis spectrum of BODIPY

Table 1. Photophysical parameters of coumarins (**C1**-**C3**) and coumarin-BODIPY dyads (**B1**-**B3**).

	λ^{abs} (nm, max)	log ε	λ^{ems} (nm, max)	Δ_{Stokes}, (nm)	Φ_F	τ_F (ns)
C1	340	4.91	422	82	0.39	3.02
C2	340	5.01	420	80	0.56	3.08
C3	380	5.04	518	138	0.60	5.09
B1	502	4.90	512	10	0.55	2.31
B2	502	4.67	511	9	0.54	2.29
B3	502	4.84	514	12	0.39	2.22

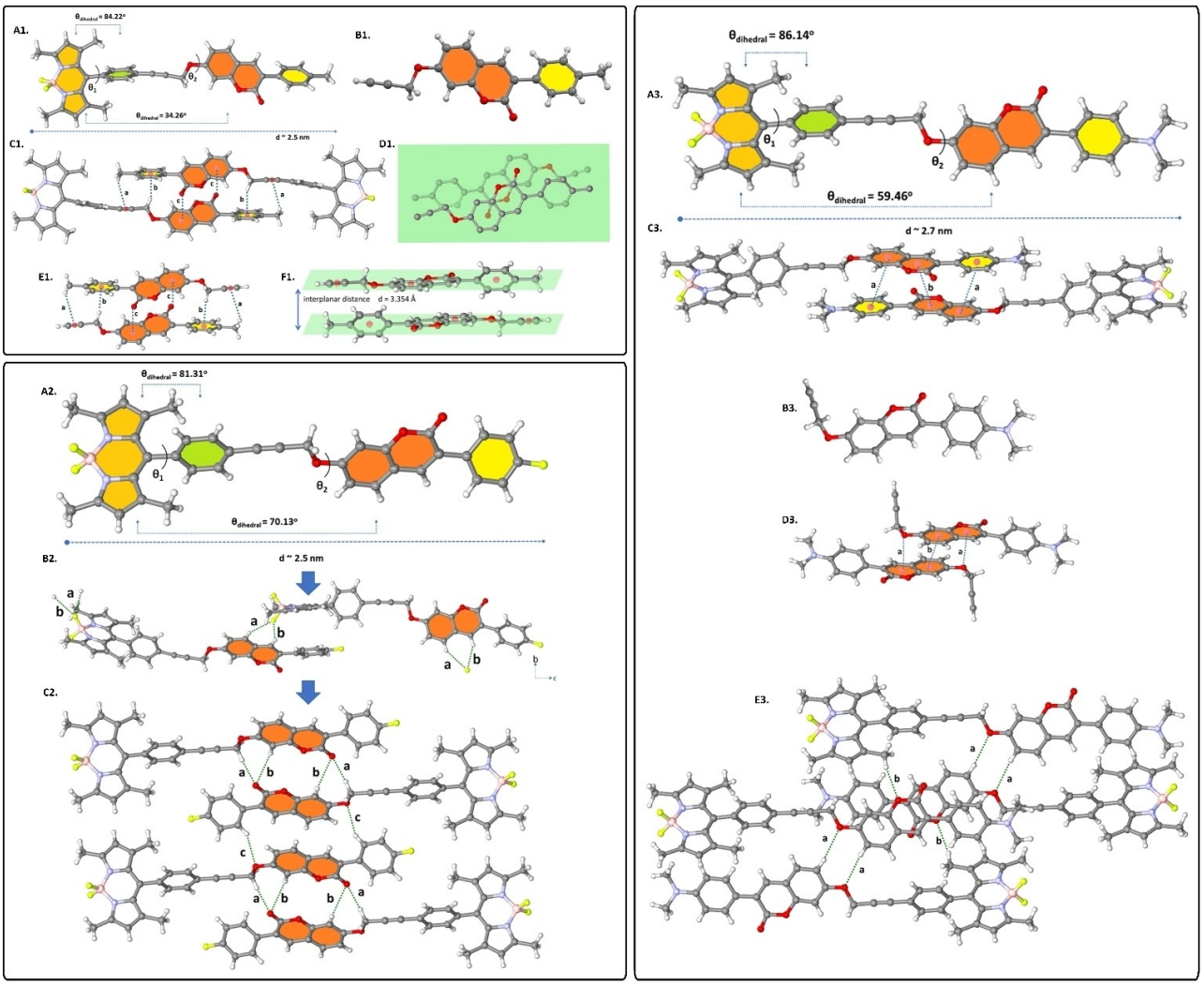

Figure 1. (A1) Ball-stick style drawings of the molecular structures showing the corresponding inter-ring dihedral angles between the planes in **B1** compound. (B1) Perspective view of molecular structure of **C1**. (C1) The intermolecular interactions in **B1** (a: C–H···π(ethynyl), $d_{(H\cdots\pi)}=2.951$ Å, b: C–H···π(phenyl); $d_{(H\cdots\pi)}=2.655$ Å, c: –C=O(δ^-)···π(phenyl), $d_{(C=O(\delta^-)\cdots\pi}=3.602$ Å. (D1), (E1), (F1) Representations of pairs of coumarin molecules (**C1**) (a: C–H···π(ethynyl), $d_{(H\cdots\pi)}=3.543$ Å, b: C–H···π(phenyl); $d_{(H\cdots\pi)}=2.732$ Å, c: –C=O(δ^-)···π(phenyl), $d_{(C=O(\delta^-)\cdots\pi}=3.320$ Å). (A2) Ball-stick style drawings of the molecular structures showing the corresponding inter-ring dihedral angles between the planes in **B2** compound. (B2) The intermolecular C–H···F interactions in **B2** (a: $d_{(H\cdots F)}=2.608$ Å, b: $d_{(H\cdots F)}=2.351$ Å). (C2) The intermolecular C–H···O interactions in **B2** (a: $d_{(H\cdots O)}=2.189$ Å, b: $d_{(H\cdots O)}=2.711$ Å, c: $d_{(H\cdots O)}=2.643$ Å). (A3) Ball-stick style drawings of the molecular structures showing the corresponding inter-ring dihedral angles between the planes in **B3**. (B3) Molecular structure of **C3** compound. (C3) The intermolecular π ···π interactions in **B3** (a: $d_{(\pi\cdots\pi)}=3.858(4)$ Å, b: $d_{(\pi\cdots\pi)}=3.518(4)$ Å). (D3) Representations of pairs of coumarin molecules (**C3**) arranged in a slipped stacked through –C=O(δ^-)···π(coumarin) interactions (a: $d_{(C=O(\delta^-)\cdots\pi}=3.195$ Å, b: $d_{(\pi\cdots\pi)}=3.649$ Å). (E3) The intermolecular C–H···O interactions in **B3** (a: $d_{(H\cdots O)}=2.589$ Å, b: $d_{(H\cdots O)}=2.483$ Å).[57]

compounds, is observed at 502 nm and it consistent with the literature.[34] The absorption wavelengths of **B1** and **B2** from the coumarin moieties are observed at 340 nm, while the absorption wavelength of **B3** from the coumarin moiety is observed at 380 nm. This difference is due to the effect of the strong electron donor $-NMe_2$ group on the coumarin ring. There was no significant difference in the UV-Vis spectra in different studied solvents, indicating that strong solvatochromism did not occur for all three studied coumarin-BODIPY dyads. The UV-Vis spectra of the dyads **B1**-**B3** at the different concentration changing from 1 to 10 μM were examined and no aggregation was observed for these molecules in this concentration range. The molar absorption coefficient (logε) values were obtained as 4.90, 4.67 and 4.84, respectively (Figure 2).

Fluorescent emissions were recorded in dichloromethane for coumarin derivatives (**C1**-**C3**) and coumarin-BODIPY dyads (**B1**-**B3**). The fluorescence quantum yields were calculated as 0.39, 0.56, and 0.60 for coumarin (**C1**-**C3**) and 0.55, 0.54, 0.39 for coumarin compounds (**C1**-**C3**) using quinine sulfate ($\varphi_F=0.546$ in 0.5 M H_2SO_4) and for coumarin-BODIPY compounds (**B1**-**B3**) using rhodamine 6G ($\varphi_F=0.95$ in ethanol) as standards, respectively.

For coumarin compounds, the effect of the electron-donating groups on the lactone ring and the α-ß unsaturated carbonyl group increases the emission intensity and fluorescence quantum yield. Therefore, **C3** has the highest quantum efficiency and longest emission wavelength. However, it has been reported in the literature that emission and thus

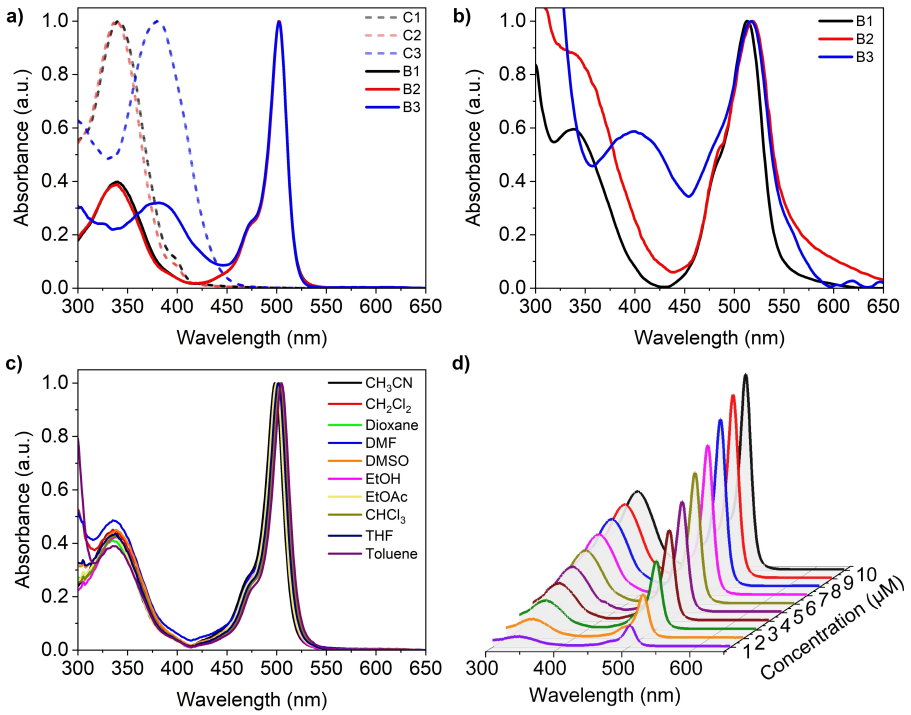

Figure 2. Comparative UV-Vis spectra of the compounds (**C1**-**C3** and **B1**-**B3**) in dichloromethane (a) and on thin films (b). UV-Vis spectra of BODIPY's (**B1**-**B3**) in ten different solvents (c) and ten concentrations in dichloromethane (d).

quantum yield decrease due to photoinduced electron transfer (PET) in structures where such strong electron donor groups are present together with acceptor groups such as BODIPY. **B3** is a hybrid compound consisting of donor coumarin containing a strong electron-donating -NMe_2 group and acceptor BODIPY center. For this reason, a decrease in emission intensity and quantum efficiency was observed due to the above-mentioned effect. On the other hand, it was observed that the electron-withdrawing fluorine and weak electron-donating methyl group in the target two coumarin-BODIPY compounds (coumarin-BODIPY containing fluorophenyl and tolyl groups) did not have a significant effect on BODIPY emission in terms of either emission intensity or quantum yield. Considering the thin film emissions, it was determined that **B1** and **B2** emitted at 533 nm, and **B3** emitted at 572 nm. The extra emission band given by **B3** at 572 nm is thought to be the emission band resulting from the π-π packaging of this molecule, and it has been reported that thin-film emissions give new secondary or tertiary emission bands at higher wavelengths in molecules that make this type of π-π packing (Figure 3b).[35]

The excited state lifetimes (τ_F) of the starting coumarins (**C1**-**C3**) and coumarin-BODIPY dyads (**B1**-**B3**) were measured in dichloromethane using time-dependent single photon counting method (Figure 4). It was observed that coumarin compounds have longer fluorescence lifetimes than coumarin-BODIPY derivatives (Table 1). Among the coumarins, **C1** containing the tolyl group has the shortest fluorescence lifetime (3.02 ± 0.005 ns). The fluorescence lifetime of **C2** containing

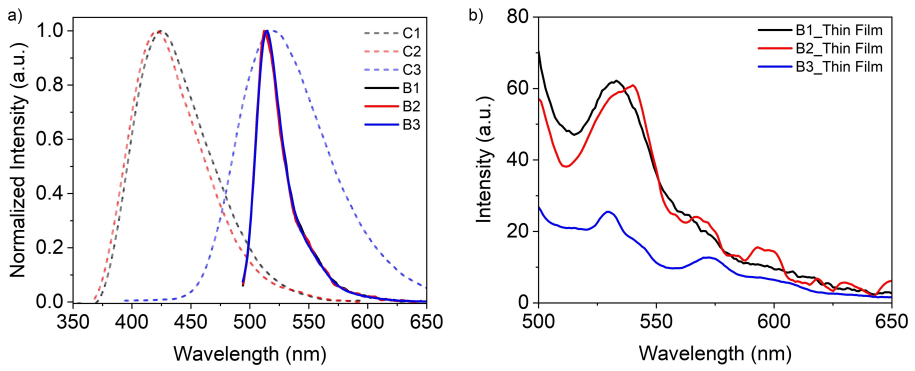

Figure 3. The fluorescence spectra of coumarin-BODIPY dyads (**B1**-**B3**) in dichloromethane (a) and on thin films (b). (Concentrations for PL measurements 1×10^{-6} M; λ^{em}_{start} =340 nm for **C1** and **C2**, λ^{em}_{start} =380 nm for **C3**, λ^{em}_{start} =480 nm for **B1**-**B3**).

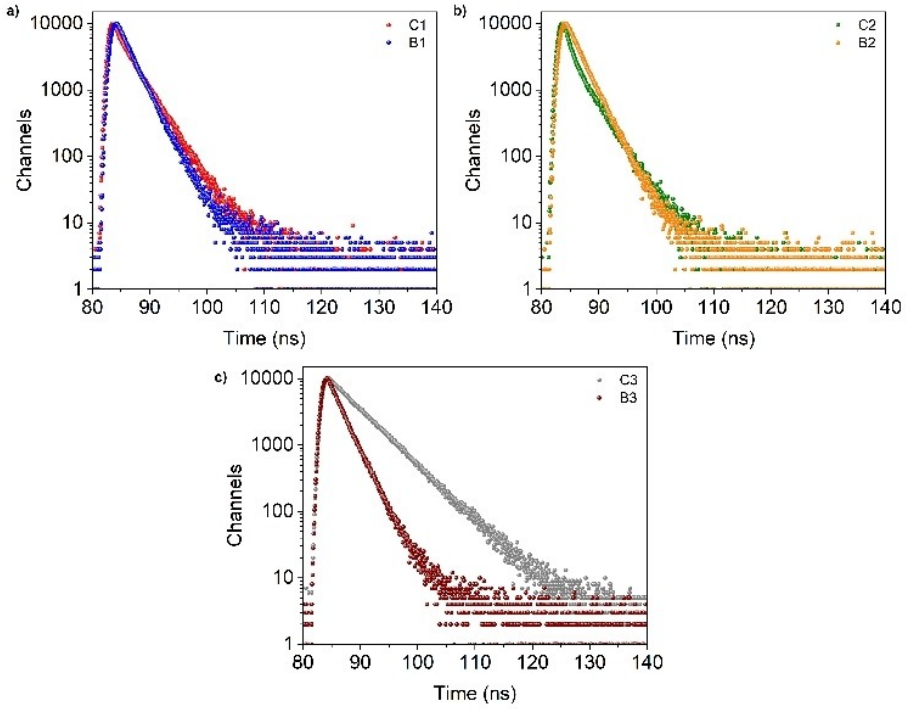

Figure 4. Time-correlated single-photon counting (TCSPC) trace for **C1**-**B1** (a), **C2**-**B2** (b) and **C3**-**B3** (c) in dichloromethane. (λ_{em}^{all} =390 nm; λ_{exc}^{C1} =422 nm, λ_{exc}^{C2} =420 nm, λ_{exc}^{C3} =518 nm, λ_{exc}^{B1} =512 nm, λ_{exc}^{B2} =512 nm and λ_{exc}^{B3} =514 nm).

electron acceptor (fluorine) group was slightly increased compared to **C1** (3.08 ± 0.010 ns). The fluorescence lifetime of coumarin **C3** bearing a strong electron donor group (dimethylamino) was considerably increased (5.09 ± 0.006 ns) compared to **C1** and **C2**. The strong electron-donating -NMe_2 group causes a higher fluorescence lifetime for **C3** than its counterparts. On the other hand, in coumarin-BODIPY dyes (**B1**-**B3**), the fluorescence lifetimes were shortened in correlation with the addition of fluorophore coumarins to the structure.

The fluorescence properties of the coumarin-BODIPY dyads (**B1**-**B3**) were measured in dichloromethane by both steady-state and time-resolved fluorescence techniques. Fluorescence spectra of the compounds **B1** and **B2** were investigated at excitation wavelengths of 340 and 480 nm, in dichloromethane, respectively and unlike **B1** and **B2**, **B3** was excited at both 380 and 480 nm due to red-shifted **C3** absorbance (Figure 5). It was demonstrated by experimental and theoretical studies that the Forster energy transfer mechanism is responsible for the energy transfer from the high energy donor coumarin units to the low energy acceptor BODIPY core. Therefore, coumarin-BODIPY dyads form a potential donor-acceptor pair for energy transfer.

To obtain more information on energy transfer, the emission spectra of the starting coumarins and the coumarin-BODIPY dyads were measured under the same conditions (1×10^{-6} M in dichloromethane). Fluorescence maximum peaks were observed at 514 and 513 nm when excited at 480 nm from BODIPY part for **B1** and **B2**, respectively. When excited from 340 nm, the fluorescence maximum peaks were observed again at 514 and 513 nm, but the emission intensities decreased. For **B3**, when excited this compound from BODIPY part at 480 nm, the fluorescence maximum peak was observed at 514 nm. When excited this compound from 380 nm, the fluorescence maximum peak was observed at 514 nm and the emission intensities decreased again. This indicated that the energy transfer occurred from the coumarin group to BODIPY ring because the compounds did not produce any emissions when excited at 340 or 380 nm.

Electrochemistry

Electrochemical characterizations of **B1**-**B3** were carried out by CV and DPV techniques. The oxidation-reduction mechanisms of **B1**-**B3** were elucidated by referencing the CV voltammograms of the initial compounds (Figure S27). Accordingly, the oxidation peak of the BODIPY core was observed at approximately 1.25 V ($E_{1/2}$ = 1.38 V, $E_{1/2}$ = 1.30 V, $E_{1/2}$ = 1.33 V vs Ag/AgCl, respectively), reduction peak of the BODIPY core was observed at approximately −1.0 V ($E_{1/2}$ = −0.91 V, $E_{1/2}$ = −0.98 V, $E_{1/2}$ = −0.94 V vs Ag/AgCl, respectively) and finally oxidation of coumarin moiety was observed at approximately −1.5 V in all coumarin-BODIPY molecules during the anodic and cathodic scan. The oxidation peak of the BODIPY core shifted from 1.34 to 1.41 V due to the electron-withdrawing effect of the fluorine atom in the meso position of the **B2** structure. In addition, the oxidation of the electron donor *N*,*N*-dimethylamino moiety in the C-3 position of the coumarin was observed as an extra peak at 0.96 V ($E_{1/2}$ = 0.93 vs Ag/AgCl) at the CV of **B3**.

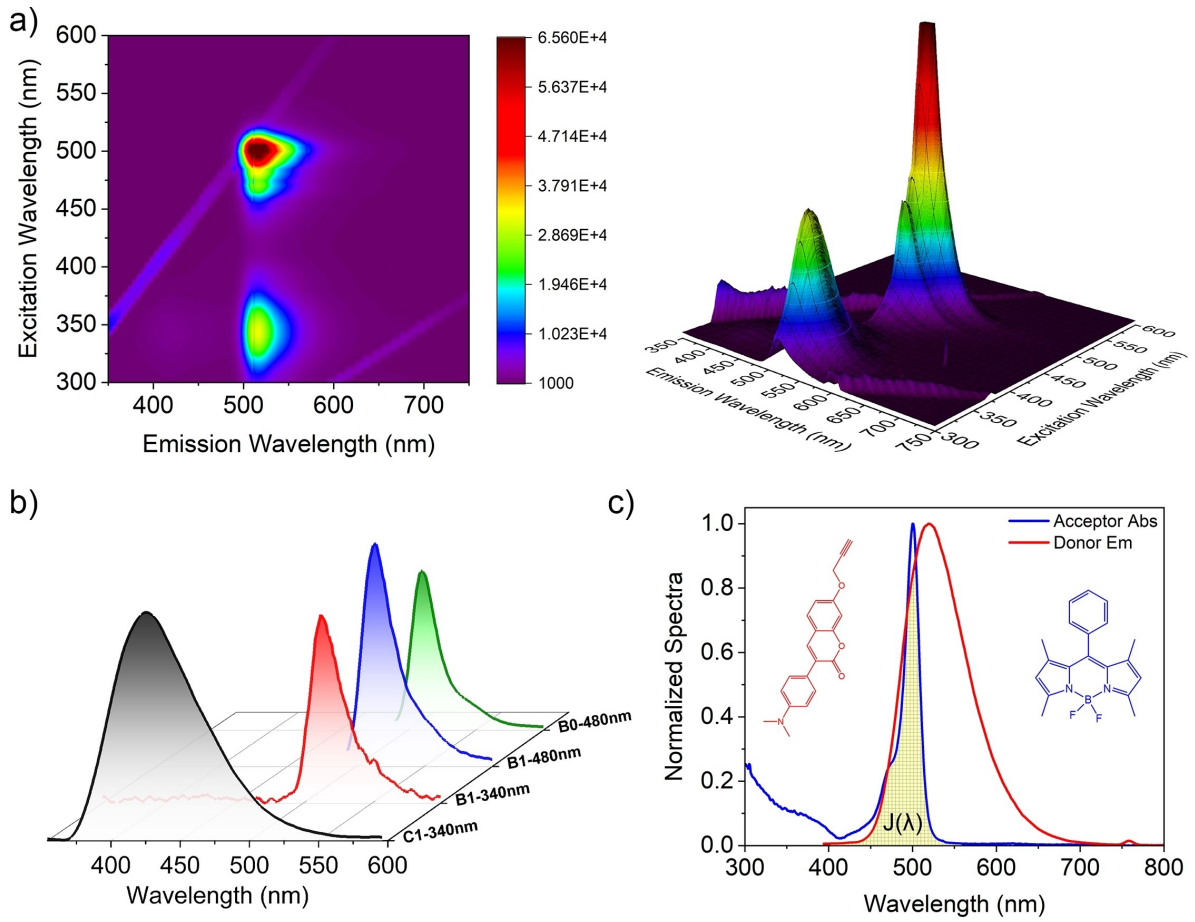

Figure 5. a) The 2D and 3D contour fluorescence Em/Ex spectra of **B2** in dichloromethane. b) Overlapping emission spectra of excited coumarin-BODIPY (**B1**), coumarin (**C1**) and reference acceptor (**B0**) compounds from different wavelengths in dichloromethane. c) Spectral overlap density display of donor coumarin (**C3**) and acceptor reference BODIPY (**B0**) compounds in dichloromethane. (Concentrations for UV-Vis measurements 1×10^{-5} M and for PL measurements 1×10^{-6} M).

Considering the reduction potential of BODIPY, a slightly positive shift at the reduction potential was observed depending on the electron density. The HOMO-LUMO energy levels of all compounds were calculated from DPV, and the band gaps were found as 2.03 eV for **B1**, 2.01 eV for **B2** and 1.59 eV for **B3** (Figure 6).

Density Functional Theory Calculations

Molecular geometry optimizations of the coumarin-BODIPY compounds (**B1**-**B3**) were calculated by DFT method and molecular structures were obtained from crystal information file (cif) before computation.

The energy levels of molecular orbitals of coumarin-BODIPY compounds (**B1**-**B3**) are shown in Figure 7. While HOMO and LUMO energy levels and band gaps were very close to each other for **B1** and **B2** compounds, the HOMO energy level increased, and the band gap narrowed for **B3** due to containing a dimethylamino donor group in its structure. The reason for the increased HOMO energy level for **B3** is that a donor group, dimethylamino, donates electrons to the coumarin ring and the charge density migrates from coumarin to the BODIPY core via acetylene linker. The calculated band gaps are 2.97 eV for **B1**, 2.96 eV for **B2** and 2.51 eV for **B3** and they are in correlation with the experimental band gaps (Figure 7).

The electronic contributions and positions of molecular orbitals provide important information about charge transfer. For **B1** and **B2** compounds, HOMO and LUMO orbitals are located on BODIPY, while LUMO + 1 orbitals are located on coumarin, which carries acceptor groups (fluorine and methyl). On the other hand, the HOMO orbitals are located in the coumarin-bearing donor dimethylamino subunit, and the LUMO and HOMO-1 orbitals are located in the center of BODIPY, due to the intramolecular charge transfer of the electron-rich *N*,*N*-dimethylamino group for **B3**. In the literature, there are many examples on strong electron donor groups such as *N*,*N*-dimethyl, *N*,*N*-diphenyl etc. show intramolecular charge transfer (ICT), especially in BODIPY structures.

Contributions of various parts of HOMOs and LUMOs of molecules were calculated using the GaussSum software. The coumarin-BODIPY compounds were subdivided into two parts, (coumarin, and BODIPY), and their corresponding percentage contributions are shown in Figure 8. In all molecules, the

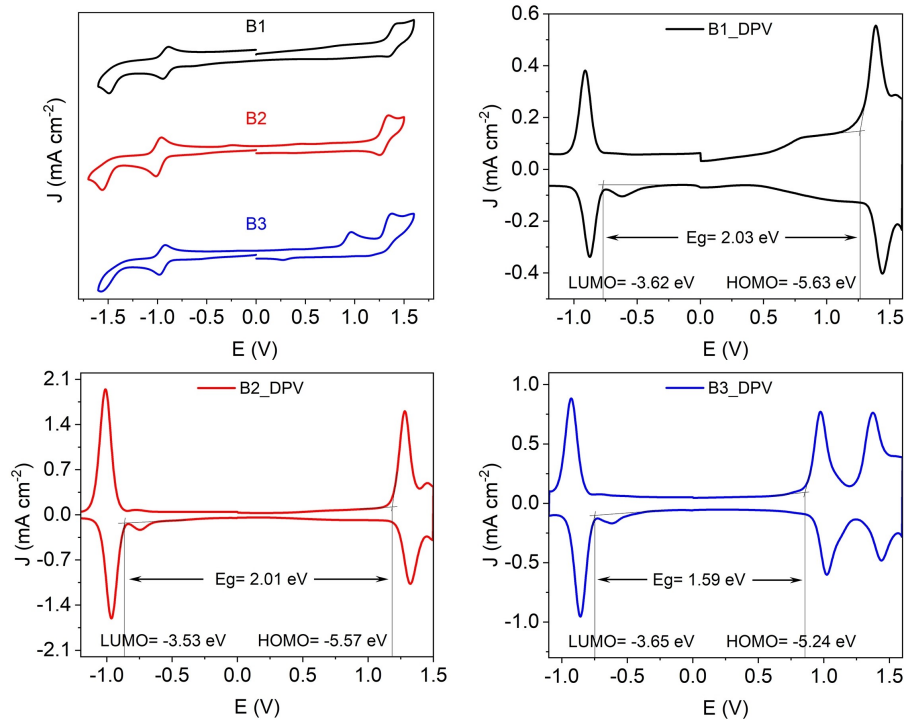

Figure 6. The cyclic voltammetry (CV) and differential pulse voltammetry (DPV) spectra of **B1**-**B3** on GCE in DCM/$TBAPF_6$ at 100 mV s^{-1} vs. Ag/AgCl.

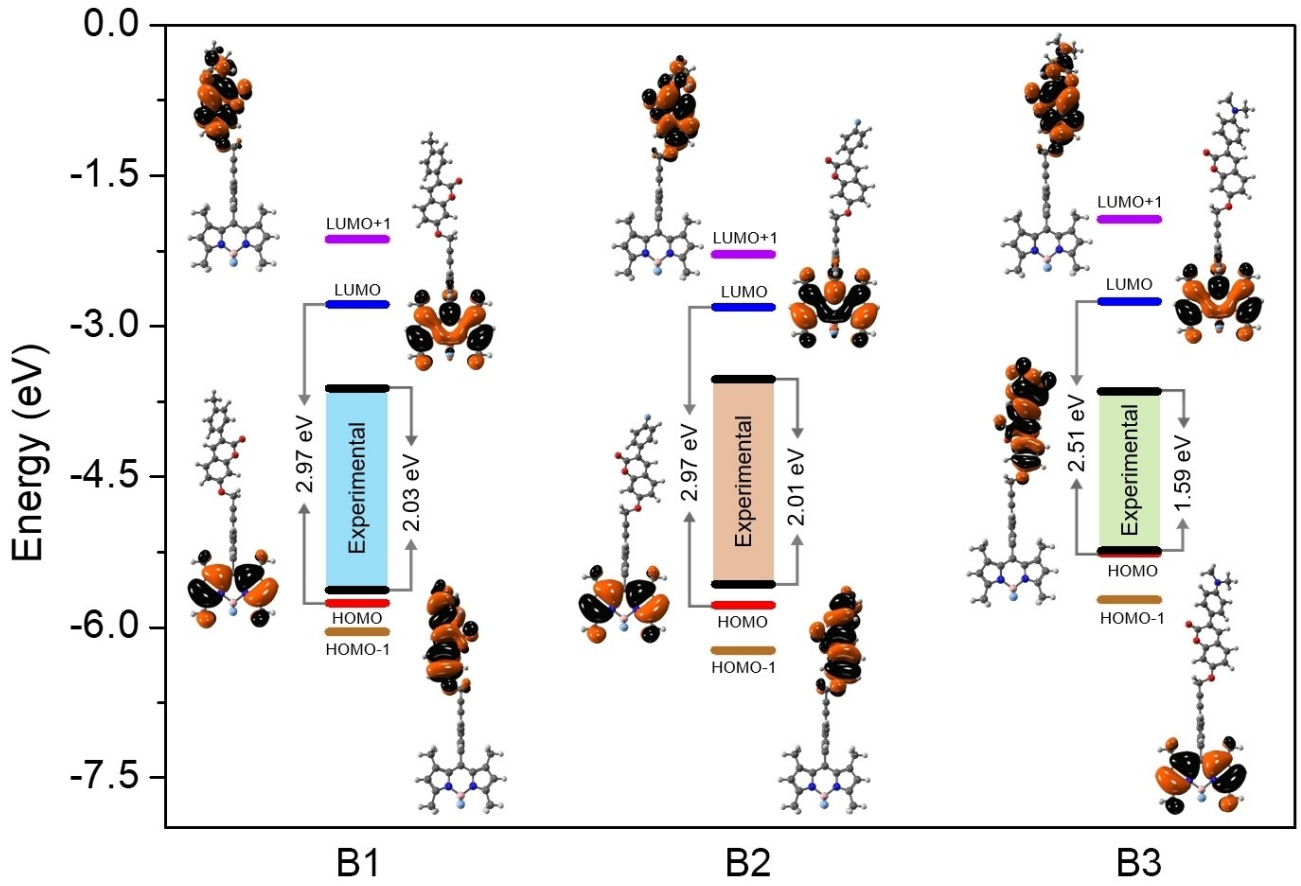

Figure 7. The experimental and theoretical molecular orbital energy diagram of the coumarin-BODIPY's (**B1**-**B3**).

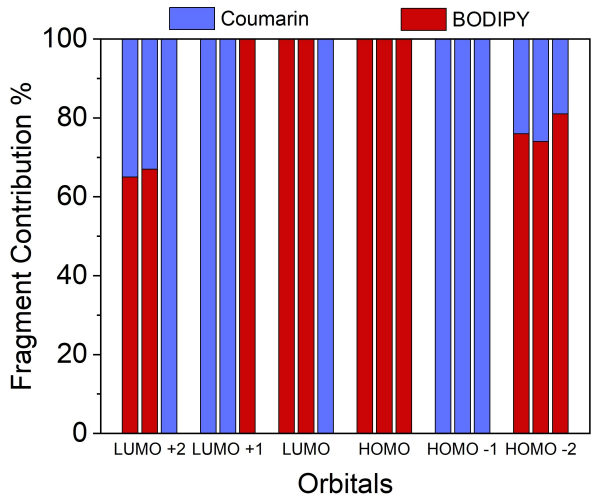

Figure 8. Molecular orbital composition (%) of the three highest occupied and three lowest unoccupied molecular orbitals.

BODIPY unit appears to contribute 100% to HOMO. Coumarins with weak electron acceptor groups contributed 100% to LUMO + 1, while coumarins with strong electron donor groups contributed 100% to LUMO. All coumarins contributed 100% to HOMO-1 without exception. For **B1** and **B2**, the BODIPY unit contributed 100% to LUMO, while for **B3** it contributed 100% to LUMO + 1.

Conclusion

In conclusion, the effects on the FRET activity of electron withdrawing and electron donating groups on the coumarin-BODIPY dyads structures was investigated in this study. Electrochemical and optical characterizations were supported by DFT calculations, and it was observed that all molecules showed bipolar behavior thus the charges at ground state and excited state with the completely separated with each other. In addition, it was concluded that coumarin-BODIPY dyads, whose thin films were prepared, were highly effective on crystallinity. As 3D fluorescence and DFT results were examined, it was observed that there was energy transfer from the coumarin molecule to the BODIPY center by the FRET mechanism. In addition, these molecules have potential for medical treatment such as biosensors and tumor screening as well as optoelectronic applications.

Experimental Section

Materials and Equipment

4,4′-Difluoro-8-(4-iodo)-phenyl-1,3,5,7-tetramethyl-4-bora-3a,4a-diaza-s-indacene, 7-hydroxy-3-(p-tolyl)coumarin and 7-hydroxy-3-(p-fluorophenyl)coumarin were synthesized according to procedures giving in the literature.[36–38]

The starting materials: 4-Iodobenzaldehyde, 2,4-dimethylpyrrole, 2,3-dichloro-5,6-dicyano-1,4-benzoquinone, boron trifluoride diethyl etherate, 2,4-dihydroxybenzaldehyde, 4-fluorophenylacetic acid, *p*-tolylacetic acid, *N*,*N*-(dimethylamino)phenylacetic acid, propargyl bromide, $Pd(PPh_3)_2Cl_2$, copper(I) iodide, sodium acetate, potassium carbonate and all solvents were purchased from Sigma-Aldrich, Merck KGaA.

The progress of the reactions and the purity of the products were checked by thin-layer chromatography (TLC) technique. FT-IR spectra were recorded on the Perkin Elmer Spectrum 100 FT-IR Spectrometer with ATR capability. ^{1}H-NMR, ^{13}C-NMR, ^{11}B-NMR, and ^{19}F-NMR spectra were recorded on Bruker Avance III 500 spectrometer in deuterated chloroform ($CDCl_3$). Electronic absorption spectra (UV-Vis) were recorded on Shimadzu UV-2450 UV-Visible Spectrophotometer. Fluorescence excitation and emission spectra were recorded on the Hitachi F-7000 spectrofluorometer using a 1 cm path length cuvette at room temperature in dichloromethane. Mass spectra were recorded on Bruker Microflex LT MALDI-TOF MS spectrometer using α-cyano-4-hydroxycinnamic acid (CHCA), 2,5-dihydroxybenzoic acid (DHB) or dithranol (DIT) as the MALDI matrixes. Thermal gravimetric analysis (TGA) was carried out using a Mettler Toledo TGA/SDTA851 instrument (heating rate of 10 °C min^{-1}), and differential scanning calorimetry (DSC) measurements were performed using a Mettler Toledo DSC 821^{e} equipped with Star^{e} software (scanning rate of 10 °C min^{-1}) and operated under a nitrogen flow (50 mL min^{-1}). Atomic Force Microscopy (AFM) images were obtained in both the height and phase-contrast mode using a Digital Instruments Dimension 3000 scanning force microscope in the tapping mode. Transmission electron microscopy (TEM) was performed using a JEOL 2000CX instrument at 200 kV accelerating voltage.

Single crystal X-ray diffraction experiments were performed on a Bruker APEX II CCD using monochromatized Mo-Kα X-radiation (λ = 0.71073 Å). Indexing, data collection, data reduction[39] and absorption correction[40] were carried out using APEX2.[41] All crystal structures were solved using SHELXT[42] and then refined by full-matrix least-squares refinements on F^2 using the SHELXL[43] in Olex2 Software[44] Package. The aromatic and aliphatic C-bound H atoms were positioned geometrically and refined using a riding mode. Crystal structure validations, geometrical calculations and drawings were performed using Platon[45] and Mercury[46] software. Additional crystallographic data with CCDC reference numbers 2214943 (**C1**), 2173565 (**B1**), 2173566 (**B2**), 2214944 (**C3**), and 2173585 (**B3**) have been deposited within the Cambridge Crystallographic Data Center *via* www.ccdc.cam.ac.uk/deposit.

To understand electrochemical properties and calculation of band gap energy levels, cyclic voltammetry (CV) was carried out using a three-electrode cell system comprising a glassy carbon electrode as the working electrode, and a platinum wire and saturated calomel electrode (SCE) as counter and reference electrodes, respectively. Also, these measurements were recorded at Dropsens μStat 400 Bipotentiostat/Galvanostat instrument in dichloromethane, containing 0.1 M n-Bu_4NPF_6 as the supporting electrolyte recorded at a scan speed of 100 mV s^{-1}.

As an important photophysical parameters, fluorescence quantum yields (φ_F) are determined by the comparative method according to Equation (1):

$$\phi_F = \phi_{F(Std)} \frac{F \cdot A_{Std} \cdot n^2}{F_{Std} \cdot A \cdot n^2_{Std}} \quad (1)$$

where F and F_{Std} are the areas under the fluorescence curves of **B1**-**B3** and the standard, respectively. A and A_{Std} are the respective

absorbance of the **B1-B3** and standard at the excitation wavelengths, respectively. n^2 and n^2_{Std} are the refractive indices of dichloromethane used for the sample and standard, respectively. Rhodamine 6G ($\phi_F = 0.95$ in ethanol)[47] for BODIPY derivative and quinine sulfate ($\phi_F = 0.546$ in 0.5 M H_2SO_4)[48] were employed as standard compounds in this study. The absorbances of the studied **B1**-**B3** and the standard Rhodamine 6G were kept *ca.* 0.05 at the excitation wavelength.

Fluorescence lifetime (τ_F) was measured in dichloromethane with appropriate exponential calculations by Horiba-Jobin-Yvon-SPEX Fluorolog 3-2iHR that has Fluoro Hub-B Single Photon Counting Controller. The signals were recorded by the TCSPC module. For that purpose, a NanoLED (390 nm) was used for the excitation source.

Density Functional Theory (DFT)[49] was used to investigate molecular structures and molecular properties. Molecular structures of the investigated molecules were optimized by Gaussian16[50] and visualized by GaussView 6.0.[51] The B3LYP functionals[52–54] were used for DFT with the 6-31 + G(d,p) basis set. True minimum natures of the optimized structures were verified with all positive frequencies. Solvent effects were investigated using the Polarizable Continuum Model (PCM)[55,56] in the ground state as implemented in Gaussian16.

Synthesis

General synthesis of alkynated-coumarins

1.10 g (3.90 mmol) 7-hydroxy-3-(*p*-tolyl) coumarin, 1.00 g (3.90 mmol) 7-hydroxy-3-(p-fluorophenyl) coumarin or 1.09 g (3.90 mmol) 7-hydroxy-3-(*p*-*N*,*N*-dimethylaminophenyl) coumarin and 0.51 g (4.35 mmol) or 0.51 g (4.29 mmol) propargyl bromide were dissolved in 30 mL DMF and 0.82 g (5.94 mmol) or 0.80 g (5.85 mmol) anhydrous K_2CO_3 was added by proportionally within 30 minutes and the reaction mixture was stirred and heated at 65 °C under argon atmosphere at around 2 days. At the end of this time, the reaction mixture is poured into an ice-water solution, and the obtained solid was filtered and washed with water. The crude product was purified by column chromatography on silica gel using dichloromethane as an eluent.

7-Propynoxy-3-(p–tolyl) coumarin (C1)

Chemical formula: $C_{19}H_{14}O_3$; Yield: 0.98 g (85.1 %); FT-IR (ν_{max}/cm^{-1}): 3240 (C≡C–H), 3073–3038 (Ar–CH), 2946–2858 (Alp–CH), 2124 (C≡C), 1731 (C=O), 1605–1513 (C=C); ^{1}H-NMR ($CDCl_3$, 500 MHz, δ ppm): 7.76 (s, 1H, ArH), 7.62 (d, 2H, *J* = 8.0 Hz, ArH), 7.48 (d, 1H, *J* = 8.3 Hz, ArH), 7.28 (d, 2H, *J* = 8.4 Hz, ArH), 7.00 (s, 1H, ArH), 6.95 (dd, 1H, *J* = 8.4 and 1.4 Hz, ArH), 4.79 (s, 2H, –CH_2), 2.61 (s, 1H, C≡C–H), 2.42 (s, 3H, CH_3); ^{13}C-NMR ($CDCl_3$, 125 MHz, δ ppm): 160.9, 160.1, 163.4, 154.9, 139.2, 138.6, 132.0, 129.1, 128.8, 128.3, 125.4, 114.1, 113.2, 101.7, 56.2, 21.3, 1.04; MALDI-TOF (m/z) calculated: 290.32 for $C_{19}H_{14}O_3$, found: 290.25 as $[M]^+$.

7-Propynoxy-3-(p–fluorophenyl)coumarin (C2)

Chemical formula: $C_{18}H_{11}FO_3$; Yield: 0.92 g (80.1 %); FT-IR (ν_{max}/cm^{-1}): 3288 (C≡C–H), 3072–3034 (Ar–CH), 2971–2848 (Alp–CH), 2123 (C≡C), 1710 (C=O), 1614–1506 (C=C); ^{1}H-NMR ($CDCl_3$, 500 MHz, δ ppm): 7.77 (s, 1H, ArH), 7.70 (t, 2H, *J* = 6.1 Hz, ArH), 7.49 (d, 1H, *J* = 8.4 Hz, ArH), 7.15 (t, 2H, *J* = 7.8 Hz, ArH), 7.01 (s, 1H, ArH), 6.96 (d, 1H, *J* = 8.4 Hz, ArH), 4.80 (s, 2H, –CH_2), 2.61 (s, 1H, C≡C–H); ^{13}C-NMR ($CDCl_3$, 125 MHz, δ ppm): 163.9, 161.9, 160.0, 160.4, 155.0, 139.7, 130.9, 130.2, 128.9, 124.4, 115.5, 115.4, 113.9, 113.4, 101.7, 56.2; MALDI-TOF (m/z) calculated: 294.28 for $C_{18}H_{11}FO_3$, found: 294.12 as $[M]^+$.

7-Propynoxy-3-(p-N,N-dimethylaminophenyl)coumarin (C3)

Chemical formula: $C_{20}H_{17}NO_3$; Yield: 1.01 g (81.6 %); FT-IR (ν_{max}/cm^{-1}): 3276 (C≡C–H), 3089–3037 (Ar–CH), 2978–2806 (Alp–CH), 2117 (C≡C), 1710 (C=O), 1606–1520 (C=C); ^{1}H-NMR ($CDCl_3$, 500 MHz, δ ppm): 7.69 (s, 1H, ArH), 7.65 (d, 2H, *J* = 8.7 Hz, ArH), 7.44 (d, 1H, *J* = 8.7 Hz, ArH), 6.98 (d, 1H, *J* = 2.4 Hz, ArH), 6.93 (dd, 1H, *J* = 7.8 and 2.4 Hz, ArH), 6.79 (d, 2H, *J* = 8.8 Hz, ArH), 4.78 (s, 2H, –CH_2), 3.02 (s, 6H, $N(Me)_2$, 2.60 (s, 1H, C≡C–H); ^{13}C-NMR ($CDCl_3$, 125 MHz, δ ppm): 161.2, 159.6, 154.5, 150.6, 136.8, 129.2, 128.4, 125.4, 122.5, 114.5, 113.0, 112.0, 101.6, 56.2, 40.4; MALDI-TOF (m/z) calculated: 319.36 for $C_{20}H_{17}NO_3$, found: 319.06 as $[M]^+$.

General synthesis of coumarin-BODIPY dyads

50 mg (0.111 mmol) 4,4-difluoro-8-(4-iodophenyl)-1,3,5,7-tetramethyl-4-bora-3a,4a-diaza-s-indacene and 32.2 mg, (0.111 mmol) 7-propynoxy-3-(*p*-tolyl)coumarin (**C1**), 32.6 mg, (0.111 mmol) 7-propynoxy-3-(*p*-fluorophenyl)coumarin (**C2**) or 35.4 mg (0.111 mmol) 7-propynoxy-3-(*p*-*N*,*N*-dimethyl-aminophenyl)coumarin (**C3**) were dissolved in 5 mL THF–2 mL Et_3N solvent mixture under argon atmosphere and stirred ca. 30 min. After this time, $Pd(PPh_3)_2Cl_2$ and CuI were added to the reaction mixture as catalysts and this mixture was stirred at around 12 h under an argon atmosphere. Then the reaction mixture was poured into hexane and the formed solid products were filtered. The crude product was purified by column chromatography on silica gel using hexane-dichloromethane (1 : 1) solvent mixture as an eluent.

Coumarin-BODIPY Dyad-1 (B1)

Chemical formula: $C_{38}H_{31}BF_2N_2O_3$; Yield: 35.2 mg (51.8 %); FT-IR (ν_{max}/cm^{-1}): 3079–3039 (Ar–CH), 2958–2859 (Alp–CH), 2105 (–C≡C–), 1723 (–C=O), 1613 (C=N), 1545–1512 (C=C); UV-Vis (dichloromethane, λ_{max}/nm)(logε): 338(4.50), 474(4.29), 502(4.90); ^{1}H-NMR ($CDCl_3$, 500 MHz, δ ppm): 7.79 (s, 1H, coumarin–H), 7.61 (m, 4H, ArH), 7.50 (d, 1H, *J* = 8.09 Hz, ArH), 7.28 (m, 4H, ArH), 7.09 (s, 1H, ArH), 7.01 (d, 1H, *J* = 8.09 Hz, ArH), 6.00 (s, 2H, Pyrrole–H), 5.05 (s, 2H, –CH_2), 2.57 (s, 6H, –CH_3), 2.42 (s, 3H, –CH_3), 1.41 (s, 6H, –CH_3); ^{13}C-NMR ($CDCl_3$, 125 MHz, δ ppm): 160.9, 160.4, 155.9, 155.0, 142.9, 140.5, 139.2, 138.6, 135.8, 132.6, 132.0, 131.1, 129.2, 128.8, 128.3, 125.4, 122.7, 121.4, 114.1, 113.4, 101.5, 87.3, 84.0, 56.9, 21.3, 14.6, 1.03; ^{11}B-NMR (d-$CDCl_3$, 160 MHz, δ, ppm): 0.74 (t, *J* = 33.2 Hz), ^{19}F-NMR (d-$CDCl_3$, 470 MHz, δ, ppm): −146.3 (q, *J* = 33.2 Hz –BF_2); MALDI-TOF (m/z) calculated: 612.48 for $C_{38}H_{31}BF_2N_2O_3$, found 612.40 as $[M]^+$ and 593.40 as $[M–F]^+$.

Coumarin-BODIPY Dyad-2 (B2)

Chemical formula: $C_{37}H_{28}BF_3N_2O_3$; Yield: 38.7 mg (56.5 %); FT-IR (ν_{max}/cm^{-1}): 3078–3039 (Ar–CH), 2925–2855 (Alp–CH), 2103 (–C≡C–), 1724 (–C=O), 1613 (–C=N), 1544–1509 (C=C); UV-Vis (dichloromethane, λ_{max}/nm)(logε): 336(4.26), 474(4.05), 502(4.67); ^{1}H-NMR ($CDCl_3$, 500 MHz, δ ppm): 7.79 (s, 1H, coumarin–H), 7.70 (dd, 2H, *J* = 8.4 and 5.5 Hz, ArH), 7.60 (d, 2H, *J* = 8.4 Hz, ArH), 7.51 (d, 1H, *J* = 8.4 Hz, ArH), 7.29 (d, 2H, *J* = 8.4 Hz, ArH), 7.15 (t, 2H, *J* = 8.5 Hz, ArH) 7.10 (d, 1H, *J* = 2.1 Hz, ArH), 7.03 (dd, 1H, *J* = 8.5 and 2.2 Hz, ArH), 6.00 (s, 2H, Pyrrole–H), 5.06 (s, 2H, –CH_2), 2.57 (s, 6H, –CH_3), 1.41 (s, 6H, –CH_3); ^{13}C-NMR ($CDCl_3$, 125 MHz, δ ppm): 163.9, 161.9, 160.6, 155.9, 155.1, 142.9, 140.4, 139.7, 135.8, 132.6, 131.1,

130.2, 128.9, 128.3, 124.3, 122.6, 121.4, 115.5, 113.9, 113.6, 101.5, 87.3, 83.9, 57.0, 14.6, 1.03; ^{11}B-NMR ($CDCl_3$, 160 MHz, δ, ppm): 0.74 (t, J = 32.9 Hz), ^{19}F-NMR ($CDCl_3$, 470 MHz, δ, ppm): −112.7 (s, ArF), −146.2 (q, J = 32.6 Hz, $-BF_2$); MALDI-TOF (m/z) calculated: 616.45 for $C_{37}H_{28}BF_3N_2O_3$, found 616.22 as $[M]^+$ and 597.43 as $[M-F]^+$.

Coumarin-BODIPY Dyad-3 (B3)

Chemical formula: $C_{39}H_{34}BF_2N_3O_3$; Yield: 38.4 mg (54.0 %); FT-IR (ν_{max}/cm^{-1}): 3082–3037 (Ar–CH), 2922–2847 (Alp–CH), 2109 (–C≡C–), 1714 (–C=O), 1610 (–C=N), 1528–1502 (C=C); UV-Vis (dichloromethane, λ_{max}/nm)(logε): 336(4.35), 475(4.25), 502(4.84); ^{1}H-NMR ($CDCl_3$, 500 MHz, δ ppm): 7.72 (s, 1H, coumarin–H), 7.67 (d, 2H, J = 8.5 Hz, Ar–H), 7.61 (d, 2H, J = 7.9 Hz, Ar–H), 7.48 (d, 1H, J = 8.6 Hz, Ar–H), 7.28 (m, 2H, Ar–H), 7.08 (d, 1H, J = 1.79 Hz Ar–H) 6.98 (dd, 1H, J = 8.5 and 2.4 Hz, Ar–H), 6.80 (d, 2H, J = 8.6 Hz, Ar–H), 6.00 (s, 2H, Pyrrole–H), 5.04 (s, 2H, $-CH_2$), 3.08 (s, 6H, $-CH_3$), 2.57 (s, 6H, $-CH_3$), 1.41 (s, 6H, $-CH_3$); ^{13}C-NMR ($CDCl_3$, 125 MHz, δ ppm): 163.9, 161.9, 160.6, 155.9, 155.1, 142.9, 140.4, 139.7, 135.8, 132.6, 131.1, 130.2, 128.9, 128.3, 124.3, 122.6, 121.4, 115.5, 113.9, 113.6, 101.5, 87.3, 83.9, 57.0, 14.6, 1.03; ^{11}B-NMR ($CDCl_3$, 160 MHz, δ, ppm): 0.74 (t, J = 32.9 Hz), ^{19}F-NMR (d-$CDCl_3$, 470 MHz, δ, ppm): −146.2 (q, J = 32.9 Hz, $-BF_2$); MALDI-TOF (m/z) calculated: 641.51 for $C_{39}H_{34}BF_2N_3O_3$, found 641.86 as $[M]^+$ and 622.93 as $[M-F]^+$.

Acknowledgments

The numerical calculations reported in this paper were fully performed at TUBITAK ULAKBIM, High Performance, and Grid Computing Center (TRUBA resources).

Conflict of Interests

The authors declare no conflict of interest.

Data Availability Statement

The data that support the findings of this study are available in the supplementary material of this article.

Keywords: BODIPY · cross-coupling · density functional calculations · electrochemistry · energy transfer · X-ray diffraction

[1] S. Wang, J.-H. Ye, Z. Han, Z. Fan, C. Wang, C. Mu, W. Zhang, W. He, *RSC Adv.* **2017**, *7*, 36021–36025.
[2] R. D. Mitra, C. M. Silva, D. C. Youvan, *Gene.* **1996**, *173*, 13–17.
[3] J. R. Lakowicz, *Principles of Fluorescence Spectroscopy*, Springer New York, NY, **2006**.
[4] S. A. Marras, F. R. Kramer, S. Tyagi, *Nucleic Acids Res.* **2002**, *30*, e122-e122.
[5] S. Acikgoz, G. Aktas, M. N. Inci, H. Altin, A. Sanyal, *J. Phys. Chem. B.* **2010**, *114*, 10954–10960.
[6] P. Wu, L. Brand, *Anal. Biochem.* **1994**, *218*, 1–13.
[7] A. Panniello, M. Trapani, M. Cordaro, C. N. Dibenedetto, R. Tommasi, C. Ingrosso, E. Fanizza, R. Grisorio, E. Collini, A. Agostiano, *Chem. Eur. J.* **2021**, *27*, 2371–2380.
[8] I. Chambrier, C. Banerjee, S. Remiro-Buenamañana, Y. Chao, A. N. Cammidge, M. Bochmann, *Inorg. Chem.* **2015**, *54*, 7368–7380.
[9] L.-H. Yang, D. J. Ahn, E. Koo, *Mater. Sci. Eng. C.* **2016**, *69*, 625–630.
[10] A. Gopi, S. Lingamoorthy, S. Soman, K. Yoosaf, R. Haridas, S. Das, *J. Phys. Chem. C.* **2016**, *120*, 26569–26578.
[11] A. Jalihal, T. Le, S. Macchi, H. Krehbiel, M. Bashiru, M. Forson, N. Siraj, *Sustainable Chem.* **2021**, *2*, 564–575.
[12] N. Hildebrandt, C. M. Spillmann, W. R. Algar, T. Pons, M. H. Stewart, E. Oh, K. Susumu, S. A. Diaz, J. B. Delehanty, I. L. Medintz, *Chem. Rev.* **2017**, *117*, 536–711.
[13] K. Rani, U. K. Pandey, S. Sengupta, *J. Mater. Chem. C.* **2021**, *9*, 4607–4618.
[14] Y. Ge, D. F. O'Shea, *Chem. Soc. Rev.* **2016**, *45*, 3846–3864.
[15] N. Boens, V. Leen, W. Dehaen, *Chem. Soc. Rev.* **2012**, *41*, 1130–1172.
[16] E. Antina, N. Bumagina, Y. Marfin, G. Guseva, L. Nikitina, D. Sbytov, F. Telegin, *Molecules.* **2022**, *27*, 1396.
[17] J. Fan, M. Hu, P. Zhan, X. Peng, *Chem. Soc. Rev.* **2013**, *42*, 29–43.
[18] I. Esnal, G. Duran-Sampedro, A. Agarrabeitia, J. Bañuelos, I. García-Moreno, M. Macías, E. Peña-Cabrera, I. López-Arbeloa, S. De La Moya, M. J. Ortiz, *Phys. Chem. Chem. Phys.* **2015**, *17*, 8239–8247.
[19] A. Y. Bochkov, I. O. Akchurin, O. A. Dyachenko, V. F. Traven, *Chem. Commun.* **2013**, *49*, 11653–11655.
[20] J. Banuelos, I. J. Arroyo-Córdoba, I. Valois-Escamilla, A. Alvarez-Hernández, E. Pena-Cabrera, R. Hu, B. Z. Tang, I. Esnal, V. Martinez, I. L. Arbeloa, *RSC Adv.* **2011**, *1*, 677–684.
[21] P.-P. Jia, L. Xu, Y.-X. Hu, W.-J. Li, X.-Q. Wang, Q.-H. Ling, X. Shi, G.-Q. Yin, X. Li, H. Sun, *J. Am. Chem. Soc.* **2020**, *143*, 399–408.
[22] K. Zheng, H. Chen, S. Fang, Y. Wang, *Sens. Actuators B* **2016**, *233*, 193–198.
[23] J. Ordóñez-Hernández, R. Arcos-Ramos, V. Alvarez-Venicio, V. A. Basiuk, O. González-Antonio, M. Flores-Álamo, H. García-Ortega, N. Farfán, M. del Pilar Carreón-Castro, *J. Mol. Struct.* **2021**, *1239*, 130437.
[24] H. Lee, Z. Yang, Y. Wi, T. W. Kim, P. Verwilst, Y. H. Lee, G.-i. Han, C. Kang, J. S. Kim, *Bioconjugate Chem.* **2015**, *26*, 2474–2480.
[25] Y. Bai, X. Shi, Y. Chen, C. Zhu, Y. Jiao, Z. Han, W. He, Z. Guo, *Chem. Eur. J.* **2018**, *24*, 7513–7524.
[26] P. Wang, S. Guo, H.-J. Wang, K.-K. Chen, N. Zhang, Z.-M. Zhang, T.-B. Lu, *Nat. Commun.* **2019**, *10*, 3155.
[27] Y. Zhao, Y. Zhang, X. Lv, Y. Liu, M. Chen, P. Wang, J. Liu, W. Guo, *J. Mater. Chem.* **2011**, *21*, 13168–13171.
[28] M. M. Ayhan, E. Özcan, B. Dedeoglu, Y. Chumakov, Y. Zorlu, B. Coşut, *CrystEngComm.* **2021**, *23*, 268–272.
[29] E. Özcan, B. Dedeoglu, Y. Chumakov, Y. Zorlu, B. Çoşut, M. M. Ayhan, *CrystEngComm.* **2021**, *23*, 6365–6375.
[30] D. A. Tekdaş, G. Viswanathan, S. Z. Topal, C. Y. Looi, W. F. Wong, G. M. Y. Tan, Y. Zorlu, A. G. Gürek, H. B. Lee, F. Dumoulin, *Org. Biomol. Chem.* **2016**, *14*, 2665–2670.
[31] M. Ozdemir, D. Choi, Y. Zorlu, B. Cosut, H. Kim, C. Kim, H. Usta, *New J. Chem.* **2017**, *41*, 6232–6240.
[32] B. T. Aksoy, B. Dedeoglu, Y. Zorlu, M. M. Ayhan, B. Çoşut, *CrystEngComm.* **2022**, *24*, 5630–5641.
[33] M. Ozdemir, D. Choi, G. Kwon, Y. Zorlu, B. Cosut, H. Kim, A. Facchetti, C. Kim, H. Usta, *ACS Appl. Mater. Interfaces.* **2016**, *8*, 14077–14087.
[34] J. R. Flores, G. Castruita-De León, G. Turlakov, E. Arias, I. Moggio, S. M. Montemayor, R. Torres, R. Ledezma, R. F. Ziolo, J. González-Torres, *Chem. Eur. J.* **2021**, *27*, 2493–2505.
[35] D. Tian, F. Qi, H. Ma, X. Wang, Y. Pan, R. Chen, Z. Shen, Z. Liu, L. Huang, W. Huang, *Nat. Commun.* **2018**, *9*, 2688.
[36] G. Reddy, N. Duvva, S. Seetharaman, F. D'Souza, L. Giribabu, *Phys. Chem. Chem. Phys.* **2018**, *20*, 27418–27428.
[37] N. P. Buu-hoï, B. Ekert, R. Royer, *J. Org. Chem.* **1954**, *19*, 1548–1552.
[38] M. Garazd, Y. L. Garazd, A. Ogorodniichuk, V. Khilya, *Chem. Nat. Compd.* **2009**, *45*, 158–163.
[39] Bruker, in SAINT, version 8.34 A, Vol. (Ed. Eds.: Editor), City, **2013**.
[40] Bruker, in SADABS, version2014/5, Vol. (Ed. Eds.: Editor), Bruker AXS Inc., Madison, WI, City, **2014**.
[41] Bruker, in APEX2, Version 2014.11-0, Vol. (Ed. Eds.: Editor), Bruker AXS Inc., Madison, WI, City, **2014**.
[42] G. Sheldrick, *Acta Crystallogr. Sect. A* **2015**, *71*.
[43] G. M. Sheldrick, *Acta Crystallogr. Sect. C* **2015**, *71*, 3–8.
[44] O. V. Dolomanov, L. J. Bourhis, R. J. Gildea, J. A. Howard, H. Puschmann, *J. Appl. Crystallogr.* **2009**, *42*, 339–341.
[45] A. L. Spek, *Acta Crystallogr. Sect. D* **2009**, *65*, 148–155.
[46] C. F. Macrae, I. Sovago, S. J. Cotrell, P. T. A. Galek, P. McCabe, E. Pidcock, M. Platings, S. P. Greg, J. S. Stevens, M. Towler, W. A. Peter, *J. Appl. Crystallogr.* **2020**, *1*, 226–235.

[47] D. Magde, R. Wong, P. G. Seybold, *Photochem. Photobiol.* **2002**, *75*, 327–334.
[48] D. F. Eaton, *Pure Appl. Chem.* **1988**, *60*, 1107–1114.
[49] W. Kohn, L. J. Sham, *Phys. Rev.* **1965**, *140*, A1133.
[50] M. Frisch, G. Trucks, H. Schlegel, G. Scuseria, M. Robb, J. Cheeseman, G. Scalmani, V. Barone, G. Petersson, H. Nakatsuji, X. Li, M. Caricato, A. Marenich, J. Bloino, B. Janesko, R. Gomperts, B. Mennucci, H. Hratchian, J. V. Ortiz, A. F. Izmaylov, J. L. Sonnenberg, D. Williams-Young, F. Ding, F. Lipparini, F. Egidi, J. Goings, B. Peng, A. Petrone, T. Henderson, D. Ranasinghe, V. Zakrzewski, J. Gao, N. Rega, G. Zheng, W. Liang, M. Hada, M. Ehara, K. Toyota, R. Fukuda, J. Hasegawa, M. Ishida, T. Nakajima, Y. Honda, O. Kitao, H. Nakai, T. Vreven, K. Throssell, J. Montgomery, J. Peralta, F. Ogliaro, M. Bearpark, J. Heyd, E. Brothers, K. Kudin, V. Staroverov, T. Keith, R. Kobayashi, J. Normand, K. Raghavachari, A. Rendell, J. Burant, S. Iyengar, J. Tomasi, M. Cossi, J. Millam, M. Klene, C. Adamo, R. Cammi, J. Ochterski, R. Martin, K. Morokuma, O. Farkas, J. Foresman, D. Fox, in Gaussian 16 Rev. C.01, Vol. (Ed. Eds.: Editor), City, **2016**.
[51] R. Dennington, T. A. Keith, J. M. Millam, in GaussView, Version 6, Vol. (Ed. Eds.: Editor), Semichem Inc.: Shawnee Mission, KS, USA, City, **2009**.
[52] A. D. Becke, *Phys. Rev. A.* **1988**, *38*, 3098.
[53] A. D. Becke, *J. Chem. Phys.* **1993**, *98*, 5648–5652.
[54] C. Lee, W. Yang, R. G. Parr, *Phys. Rev. B.* **1988**, *37*, 785.
[55] J. Tomasi, B. Mennucci, E. Cancès, *J. Mol. Struct.* **1999**, *464*, 211–226.
[56] J. Tomasi, B. Mennucci, R. Cammi, *Chem. Rev.* **2005**, *105*, 2999–3094.
[57] Deposition Number(s) 2214943, 2214944, 2173565, 2173566, 2173585 (for compounds **C1**, **C3**, **B1**, **B2**, **B3**) contain(s) the supplementary crystallographic data for this paper. These data are provided free of charge by the joint Cambridge Crystallographic Data Centre and Fachinformationszentrum Karlsruhe Access Structures service.

Manuscript received: March 13, 2023
Revised manuscript received: May 7, 2023
Accepted manuscript online: May 14, 2023
Version of record online: ■■, ■■

RESEARCH ARTICLES

Donor/acceptor dyads: A series of coumarin-BODIPY molecules containing electron donor and acceptor subunits were prepared using a Sonogashira cross-linking reaction. The compounds were characterized and studied using X-ray structural analysis, density functional calculations and photophysical studies, and a surface analysis investigation was also carried out.

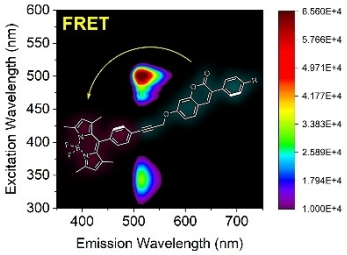

Asst. Prof. Dr. B. Köksoy, M. Özdemir, S. Altınışık, Prof. Dr. Y. Zorlu, Prof. Dr. B. Yalçın, Prof. Dr. M. Durmuş, Prof. Dr. S. Koyuncu**